

# WALL PRESSURE PROFILE AROUND CYLINDRICAL BARS IN YAWED GAS FLOW

R. G. Marino<sup>1,4</sup>, V. A. Herrero<sup>4</sup>, N. Silin<sup>2</sup>, A. Clausse<sup>3</sup>,

<sup>1</sup>*CITEFA, San Juan Bautista de La Salle 4397, 1603 Villa Martelli, Argentina*

<sup>2</sup>*CONICET and CNEA, 8400 Bariloche, Argentina.*

<sup>3</sup>*CNEA-CONICET and Universidad Nacional del Centro, 7000 Tandil, Argentina*

<sup>4</sup>*Universidad Austral, 1063 Buenos Aires, Argentina*

*Email pladema@exa.unicen.edu.ar*

*Abstract.* The distribution of wall pressures in cross flow through an array of four cylindrical tubes inclined at different angles  $30^\circ \leq \alpha \leq 90^\circ$  was experimentally studied using air at atmospheric pressure flowing at a maximum flow of 120 g/sec. The experiments show that the pressure coefficient is strongly influenced by the inclination angle, and only marginally affected by the flow rate (within the tested range). A model based on the curvature of the stream lines in the gap between bars agrees very well with the pressure coefficient at the gap.

**Keywords** — Gas flow, yawed flow, cylindrical tubes, wall pressure, boundary layer.

## I. INTRODUCTION

The separation of the boundary layer is determinant of the cross-flow resistance to the presence of solid obstacles. The problem of separation of boundary layer in gas flow received the attention of researchers for many years [1], mostly in the development of aviation industry [2]. In addition, heat exchanger technology introduced several interesting issues, such as flow around tubes and cross flow through tube bundles. Gas flow around different tube configurations has also important applications in nuclear industry, specially in advanced gas cooled reactors. Actually, a careless fluid dynamic design of fuel elements might lead to flow induced vibrations affecting normal behavior of the core structure [3]. Therefore, the generation of experimental data to support the design of fuel bundles is an important issue [4].

The flow across circular cylinders is a well known problem of fluid dynamics. A good review can be found in [5]. The issue was extensively studied in surface flow for its applications in support columns of river bridges. For internal flow, the studies were aimed mainly to heat exchangers. Fornberg [6] analyzed the incompressible cross-flow past a row of circular cylinders. Williamson [7-8] studied the three-dimensional transition of the flow behind a circular cylinder. Schewe [9] found that the drag coefficient and the vortex shedding frequency are not sensitive to the Reynolds number within the subcritical regime ( $300 < \text{Re} < 3 \cdot 10^5$ ). Numerous numerical studies of the cross-flow around cylinders were presented in 2D and 3D geometries. An updated review of these studies can be found in [10].

In several applications, such as the flow past cables, subsea pipelines, and heat exchangers, the direction of the flow is generally not perpendicular to the cylinders axis. This kind of flows can be ideally represented by a wake flow downstream of a yawed cylinder, which has been studied by a number of investigators both experimentally and numerically [10-17]. The experimental studies showed that, for an isolated long cylinder, the drag coefficient normalized

by the velocity component perpendicular to the cylinder is approximately invariant to the inclination angle (independence conjecture). In case of flow past a yawed cylinder of finite length, it was shown that the wake vortices far from the upstream end of the cylinder are approximately parallel to the cylinder. In turn, the vortices near the upstream end of the cylinder are aligned at an angle larger than the cylinder inclination.

In the present article, an experimental and theoretical study of the distribution of wall pressure around a bundle cell with three yawed tubes is presented. Although gas flow around rod bundles similar configurations were studied in the past [5, 18], pressure profiles on the wall tube were not reported in the open literature for such bundles.

## II. EXPERIMENTAL SETUP AND METHOD

The experimental setup consists of a rectangular test section that receives an air flow provided by an axial air blower. The test section hosts a cell composed of two parallel rods and two half rods embedded in the channel walls as shown in Fig. 1. The rods are mounted on a protractor so that their angle can be varied between  $90^\circ$  and  $30^\circ$  respect to the flow direction (Fig. 2). All rods are made of stainless steel with 10.86mm outer diameter and they have an overall tolerance of 0.05mm. The gap between rods is  $(2\pm 0.05)$ mm. The rods spacing and parallelism was ensured by two rod spacers located outside the test section.

The inlet flow rate to the test section was measured by means of an elliptical Pitot tube (Preso Ellipse) located on a 2" stainless steel pipe. The pipe is 1.35 m long, which ensures the flow development at the point of measurement. The Pitot tube is connected to a DP Cell Honeywell ST 300. A PT100 thermometer is used to measure the fluid temperature at the test section outlet. The flow incoming to the test section is forced through three metallic screens in order to produce a planar velocity profile and reduce turbulence levels. A settling distance of approximately 4 hydraulic diameters was taken between the last screen and the rods. The test section outlet has a length of 11 hydraulic diameters, which prevents downstream interference on the test section flow and provides a convenient location for the measurement of bulk exit conditions.

To measure the wall pressure, one of the two central rods of the test section has a 0.5mm pressure tap about the middle plane of the test section. The pressure tap diameter corresponds to  $5^\circ$  angular span; hence the angular precision is approximately  $2^\circ$ . The rod was supported so that it could be rotated around its axis to measure the different azimuthal positions. The wall pressure was measured by means of a differential pressure gauge, using the bulk static pressure at the inlet of the test section as reference. For pressure differences higher and lower than 60mbar, the Honeywell ST 300 DP Cell and the Siemens Sitrans PDS-III DP Cell are used respectively.

Measurements were performed for several gas flow rates. Flow rates were kept constant within 6% for the lowest and within 2% for the highest values. Once the steady state temperature was reached, the differential pressure between the rod wall and the inlet was recorded for different angular positions  $\theta$  ( $\theta = 0$  being the flow direction). Measurements were repeated for each rods inclination angle and flow rate.

## III. EXPERIMENTAL RESULTS

Figures 3 to 6 show the  $\theta$ -dependence of the wall pressure coefficient  $C_D$  defined as:

$$C_D(\theta) = \frac{p_w(\theta) - p_\infty}{\frac{1}{2} \rho v_\infty^2} \quad (1)$$

where  $\rho$  is the gas density,  $p_w(\theta)$  is the wall pressure at the polar angle  $\theta$ , and  $p_\infty$  and  $v_\infty$  are the inlet pressure and characteristic velocity  $v_\infty = \dot{m}/\rho_\infty A_\infty$  (being  $\dot{m}$  the mass flow rate, and  $\rho_\infty$  and  $A_\infty$  are the inlet air density and cross section area. Each graphic corresponds to measurements performed at constant flow rate, and the curves are parameterized with the inclination angle  $\alpha$ . Four flow rates were measured, namely 45, 70, 95 and 120 g/s ( $\pm 7\%$ ), corresponding to inlet velocities 12, 19, 25 and 31 m/s. The hydraulic diameter of the system is calculated as  $D_h = 2/(h^{-1} + \varepsilon^{-1})$ , where  $h$  is the channel height and  $\varepsilon$  is the gap between bars. The resulting Reynolds numbers,  $Re = v_\infty D_h / \nu$ , are 2290, 3560, 4830 and 6100, respectively.

The sources of uncertainty are the pressure difference and the flow rate measurements (see Eq. 1). The former and the latter prevail at lower and higher values of  $C_D$ , respectively. The resulting upper bound for the  $C_D$  data set is 7.5%.

In all cases, the lowest pressure is measured at  $\theta = 90^\circ$ . For  $\theta > 90^\circ$  there is a slight pressure recovery and then the pressure remains constant until  $\theta = 180^\circ$ , which is an indication of the detachment of the boundary layer. At  $\alpha = 90^\circ$  the pressure recovery occurs around  $\theta = 110^\circ$ , closer to  $\theta = 90^\circ$  than in a flow passing around an isolated bar [19]. This suggests that the presence of neighbor bars favors the detachment of the boundary layer.

As the inclination of the array increases, *i.e.*  $\alpha$  decreases, the minimum pressure at  $90^\circ$  and the back pressure at  $180^\circ$  increases. Also, the detachment point moves progressively to the rear, reaching  $\theta = 140^\circ$  at  $\alpha = 30^\circ$ . These trends are reasonable since the planar cross-section shapes tend to ellipses, which are aerodynamically better the longer is the axis parallel to the flow. Fig. 7 shows the wall pressure coefficient at the gap ( $\theta = 90^\circ$ ) and the rear of the cylinder ( $\theta = 180^\circ$ ), averaged over all measured flow rates, for different inclination angles.

#### IV. THEORETICAL ANALYSIS

Let us consider the special case of normal cross flow, *i.e.*  $\alpha = 90^\circ$ . The wall pressure at the gap between bars ( $\theta = 90^\circ$ ) can be analyzed by considering the balance of forces acting on the fluid at a small control volume located at the gap between bars as shown in Fig. 8. Consider the curvilinear system of coordinates given by the stream lines ( $\theta$ ) and the lines normal to the them ( $n$ ), the net force normal to the stream lines is [20]:

$$dF_n = \left( p + \frac{\partial p}{\partial n} dn \right) (R + dn) d\theta - pR d\theta - p dn d\theta = \frac{\partial p}{\partial n} R dn d\theta \quad (2)$$

where  $R$  is the radius of curvature of the stream lines. The mass of the control volume is  $\rho R \, dn \, d\theta$  and the centrifugal acceleration is  $\frac{v^2}{R}$ , where  $v$  is the velocity of the stream line in the control volume. Therefore by applying the second Newton law results:

$$\frac{\partial p}{\partial n} = \frac{\rho v^2}{R} \quad (3)$$

Choosing a coordinate  $y$  originated at the gap center and passing through the centers of the cylinders:

$$\frac{dp}{dy} = \frac{\rho v(y)^2}{R(y)} \quad (4)$$

From the Bernoulli equation the transversal velocity profile on the gap satisfies:

$$\rho v^2(y) = 2[p_o - p(y)] \quad (5)$$

where  $p_o$  is the stagnation pressure:

$$p_o = p_\infty + \frac{1}{2} \rho v_\infty^2 \quad (6)$$

The Bernoulli equation is valid provided that the thickness of the boundary layer is much smaller than the gap width. Mentha *et al.*[21] correlated the thickness of boundary layers in contractions including narrow gaps between cylinders. The corresponding correlations gives in our case a maximum thickness of 0.02 mm, which is neglect able compared with the 20 mm gap.

The curvature radius of the stream lines  $R(y)$  is  $a$  at the wall ( $y = \varepsilon/2$ ) and infinite at the center of the gap ( $y = 0$ ). Assuming a linear dependence of  $R^{-1}(y)$ , Eqs. **¡Error! No se encuentra el origen de la referencia.** yields:

$$\frac{dp}{dy} = -4(p_o - p) \frac{y}{a\varepsilon} \quad (7)$$

Integrating Eq. (7) gives:

$$p_o - p = C \exp\left(\frac{2y^2}{a\varepsilon}\right) \quad (8)$$

where  $C$  is an integration constant that should be determined from mass conservation considerations. The corresponding transversal velocity profile is:

$$v(y) = \sqrt{\frac{2C}{\rho} \exp\left(-\frac{y^2}{a\varepsilon}\right)} \quad (9)$$

Integrating Eq. (9) across the minimum gap gives:

$$C = \frac{1}{2} \kappa \rho \bar{v}^2 \quad (10)$$

where the average velocity in the gap between cylinders,  $\bar{v}$ , can be calculated directly by mass conservation as:

$$\bar{v} = v_\infty \frac{A_\infty}{A_g} \quad (11)$$

where  $A_\infty$  and  $A_g$  are the cross flow areas of the channel free from obstacles and at the minimum cross flow area between bars (in our case,  $A_\infty/A_g = 6.43$ ).

The coefficient  $\kappa = \left[ \int_{-1/2}^{1/2} \exp\left(-\frac{\varepsilon}{a} \xi^2\right) d\xi \right]^{-2}$  can be numerically calculated for  $\frac{\varepsilon}{a} = 0.3683$ , resulting  $\kappa = 1.066$ .

Combining Eqs. (1), (8), (10) and (11) leads to:

$$C_D(90^\circ) = 1 - \kappa \left(\frac{A_\infty}{A_g}\right)^2 \exp\left(\frac{\varepsilon}{2a}\right) \quad (12)$$

resulting  $C_D(90^\circ) = -51.7$ , which is a good approximation to the experimental value  $(-51 \pm 4)$ .

In yawed flow, *i.e.*  $30^\circ \leq \alpha < 90^\circ$ , the model can be extended considering that the horizontal cross section of the bar is an ellipse with semiminor axis  $a$  and semimajor axis  $a/\sin \alpha$ . The curvature radius of the ellipse at the gap is  $a/\sin^2 \alpha$ . Moreover, the effective transversal area at the gap,  $A_g$ , is increased a factor  $\sin^{-1} \alpha$ . The corresponding pressure coefficient at the gap for yawed flow is given by:

$$C_D(\theta = 90^\circ, \alpha) = 1 - \kappa\left(\alpha, \frac{\varepsilon}{a}\right) \left(\frac{A_\infty}{A_g}\right)^2 \sin^2 \alpha \exp\left(\frac{\varepsilon}{2a} \sin^2 \alpha\right) \quad (13)$$

where

$$\kappa\left(\alpha, \frac{\varepsilon}{a}\right) = \left[ \int_{-1/2}^{1/2} \exp\left(-\frac{\varepsilon}{a} \sin^2 \alpha \xi^2\right) d\xi \right]^{-2} \quad (14)$$

is a geometrical correction factor that is approximately 1 within the range of interest. Fig. 9 depicts the function  $\kappa(\alpha, \varepsilon/a)$ , showing that the function approaches unity as both arguments approach 0, and the maximum value is 1.18 for  $\alpha = 90^\circ$  and  $\varepsilon/a = 1$ .

The solid curve in Fig. 7 shows Eq. (13), which is in excellent agreement with the experimental data. In order to test the independence conjecture it is interesting to plot the pressure coefficient at the gap,  $C'_D$ , calculated with the velocity component perpendicular to the cylinders axis (Fig. 10). The conjecture states that  $C'_D$  is invariant to changes of the inclination angle. It can be seen that in the present case the conjecture is valid within 18%, which is a range larger than the corresponding in isolated cylinders. The curve in Fig. 10 corresponds to Eq. 13. The proposed model agrees with the experiments for inclination angles  $\alpha \geq 50^\circ$ . For lower angles, the experimental trend shows a decrease in  $C'_D$ , which can be attributed to separation of the boundary layer before  $\theta = 90^\circ$ . To appropriately describe this behavior, a three-dimensional model should be introduced.

## V. CONCLUSIONS

The polar distribution of wall pressures around a circular tube of a cell bundle in yawed air cross flow was measured for different tube inclinations and flow rates. The experiments showed that the pressure coefficient is strongly influenced by the inclination angle and only marginally affected by the flow rate (at least between 45 and 120 g/s). A model based in the curvature of the stream lines in the gap between bars was proposed to assess the lateral pressure coefficient, giving excellent results for all the measured inclination angles ( $30^\circ \leq \alpha \leq 90^\circ$ ). It was found that the pressure coefficient normalized by the velocity component perpendicular to the cylinders axis is invariant to the inclination angle within 18% tolerance.

## REFERENCES

- [1] Prandtl L., "Essentials of Fluid Dynamics", London, Blackie & Son Ltd, (1952).
- [2] Wu T. and Chen C., Taipei, Taiwan, "Laminar boundary-layer separation over a circular cylinder in uniform shear flow", *Acta Mechanica* 144, 71-82, (2000).
- [3] Kishor, K., Meher, A. and Rama, R., "Optimization of the number of spacers in a nuclear fuel bundle with respect to flow-induced vibration", *Nuclear Engineering and Design*, **236**, 2348-2355 (2006).

- [4] Fahmi, M., Hussein, M., Mohamed, S. and El-Shobokshy, S., “Experimental Investigation of the effects of extended surfaces on the performance of tube banks in cross flow”, *J. King Saud. Univ. Eng. Sci. Conf.*, Riyadh, **1**, 213-228 (1989).
- [5] Zdravkovich, M., *Flow Around Circular Cylinders: 1 Fundamentals, 2 Applications*, Oxford University Press, London (2003).
- [6] Fornberg, B., “Steady incompressible flow past a row of circular cylinders”, *J. Fluid Mech.*, **225**, 655-671 (1991).
- [7] Williamson, C., “The existence of 2 stages in the transition to three-dimensionality of a cylinder wake”, *Phys. Fluids*, **31**, 3165–3168 (1988).
- [8] Williamson, C., “The Natural and forced formation of spot-like vortex dislocations in the transition of a wake”, *J. Fluid Mech.*, **243**, 393–441 (1992).
- [9] Schewe, G., “On the force fluctuations acting on a circular cylinder in cross-flow from subcritical up to transcritical Reynolds numbers”, *J. Fluid Mech.*, **133**, 265–285 (1983).
- [10] Zhao, M., Cheng, L. and Zhou T., “Direct numerical simulation of three-dimensional flow past a yawed circular cylinder of infinite length”, *J. Fluids Structures*, **25**, 831–847 (2009).
- [11] King, R., “Vortex excited oscillations of yawed circular cylinders”, *ASME J. Fluids Eng.*, **99**, 495–502 (1977).
- [12] Thakur, A., Liu, X. and Marshall, J., “Wake flow of single and multiple yawed cylinders”, *ASME J. Fluids Eng.*, **126**, 861–870 (2004).
- [13] Chiba, K. and Horikawa, A., “Numerical solution for the flow of viscoelastic fluids around an inclined circular cylinder. II. The hydrodynamic force on a circular cylinder”, *Rheologica Acta*, **26**, 255–265 (1987).
- [14] Marshall, J., “Wake dynamics of a yawed cylinder”, *ASME J. Fluids Eng.* **125**, 97–103 (2003).
- [15] Lucor, D. and Karniadakis G., “Effects of oblique inflow in vortex-induced vibrations”, *Flow, Turbulence and Combustion*, **71**, 375–389 (2003).
- [16] Kim, T., Hodson, H. and Lu T., “On the prediction of pressure drop across banks of inclined cylinders”, *Int. J. Heat Fluid Flow* , **27**, 311–318 (2006).
- [17] Fowler, A. and Bejan, A., “Forced convection in banks of inclined cylinders at low Reynolds numbers”, *Int. J. Heat Fluid Flow*, **15**, 90–99 (1994).
- [18] Peybernès, J., “Evaluation of the forces generated by cross-flow on PWR fuel assembly”, *IAEA-TECDOC*, **1454**, 13 (2005).
- [19] White, F. M., *Fluid mechanics*, McGraw-Hill, 3rd Ed., Mexico (1996).
- [20] Shapiro, A., *The dynamics and thermodynamics of compressible flow*, **1**, 281, The Ronald Press Co., New York (1953).
- [21] Mentha, R. and Bell, J., Boundary-layer predictions for small low-speed contractions, *AIAA Journal*, **27**, 372-374 (1989).

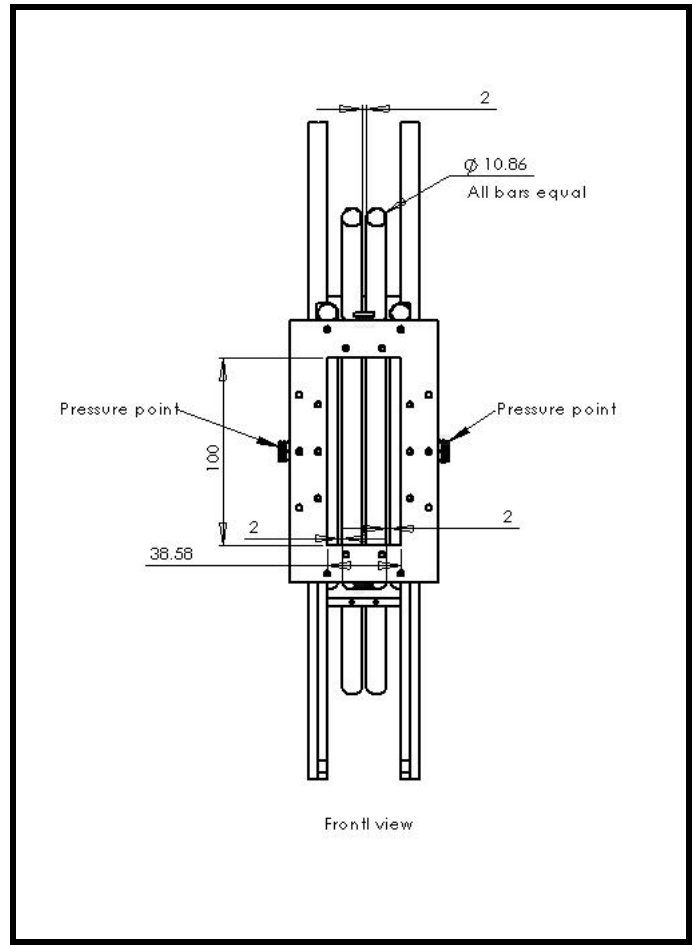


Figure 1: Cross view of the Test section (Lengths in mm)

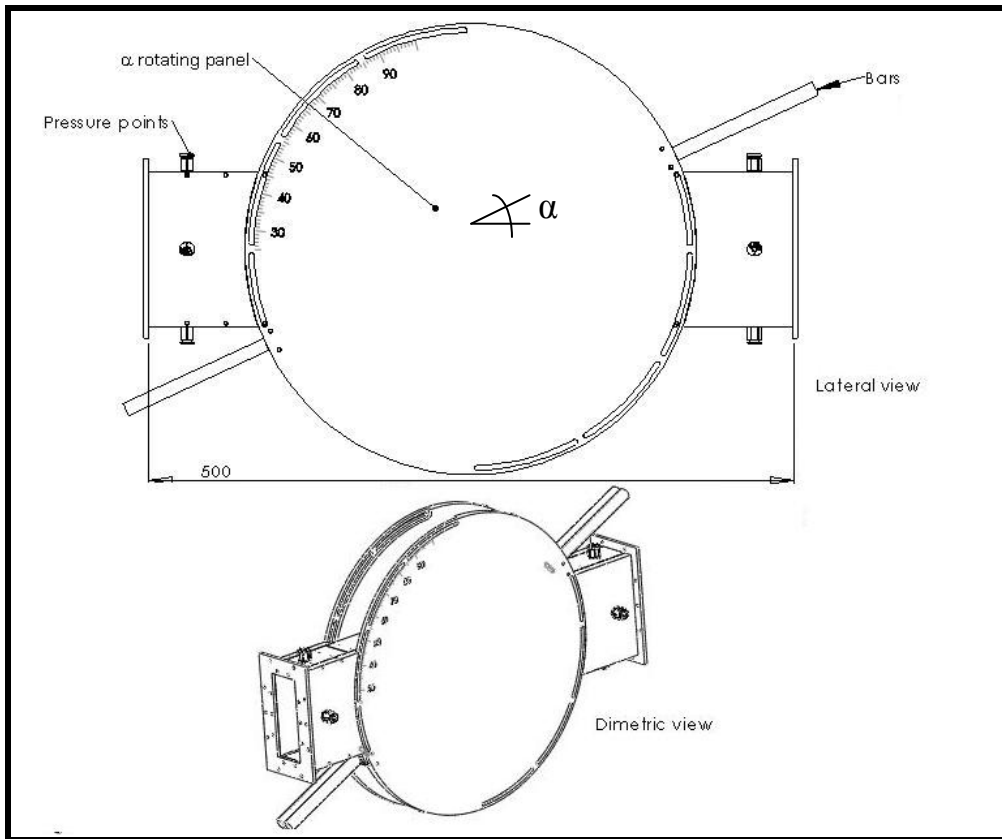


Figure 1: External view of the test section (Lengths in mm).

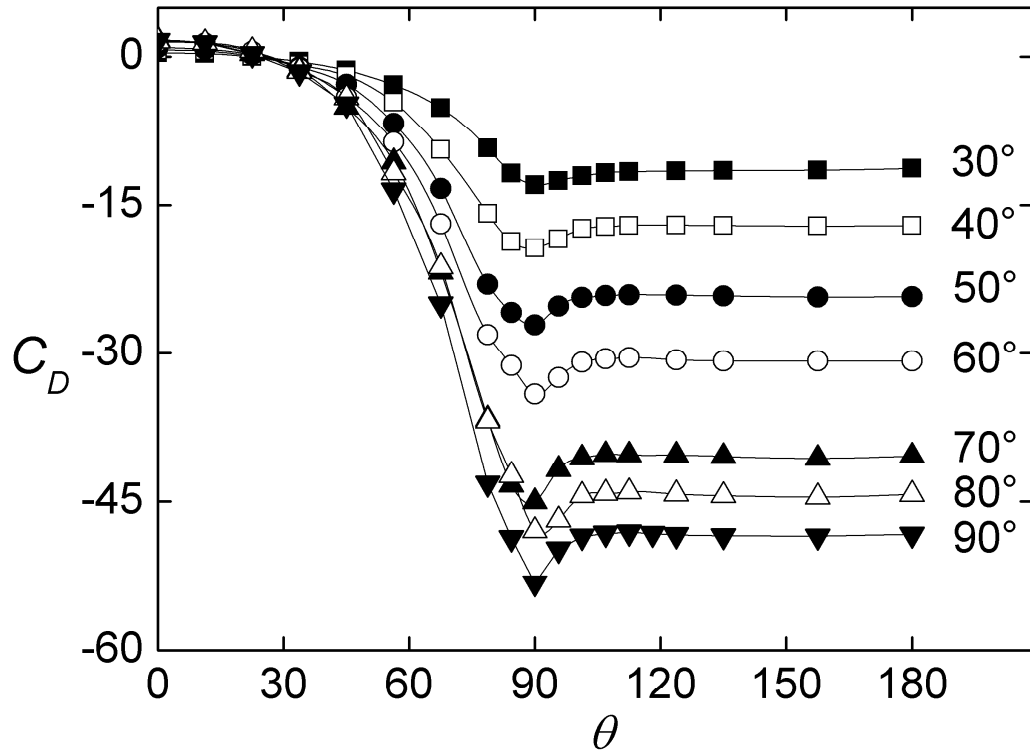


Figure 3: Polar profile of the pressure coefficient for  $Re = 2290$  (45 g/s). Each curve corresponds to inclination angles  $\alpha = 30, 40, 50, 60, 70, 80$  and  $90$  degrees respect to the incident direction.

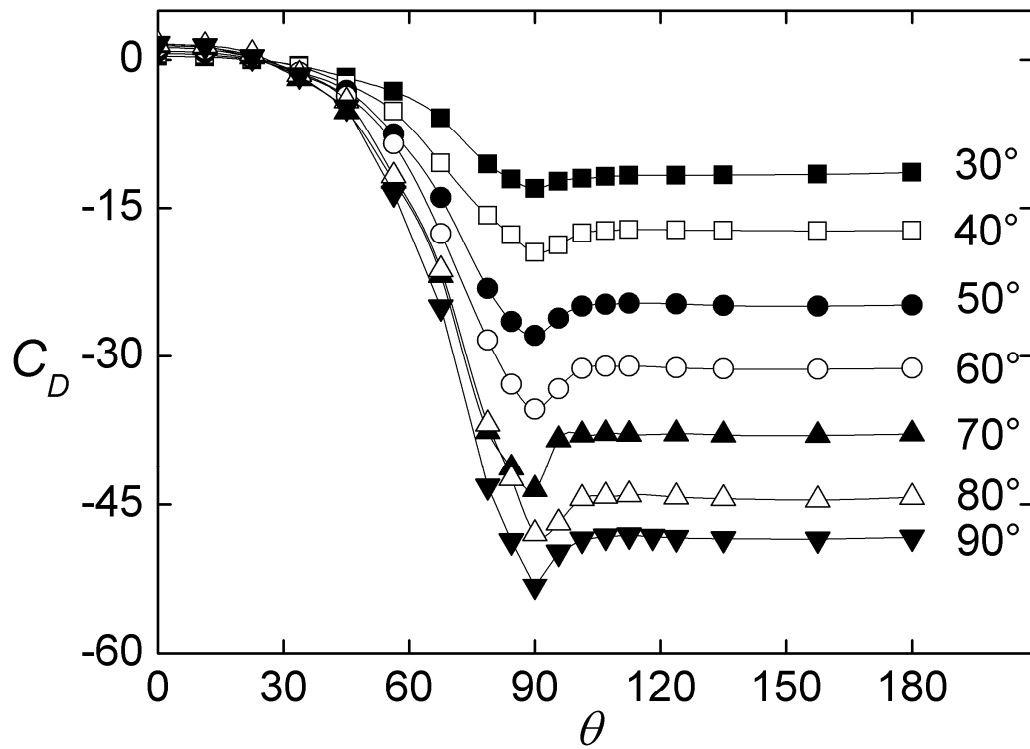


Figure 4: Polar profile of the pressure coefficient for  $Re = 3560$  (70 g/s). Each curve corresponds to inclination angles  $\alpha = 30, 40, 50, 60, 70, 80$  and  $90$  degrees respect to the incident direction.

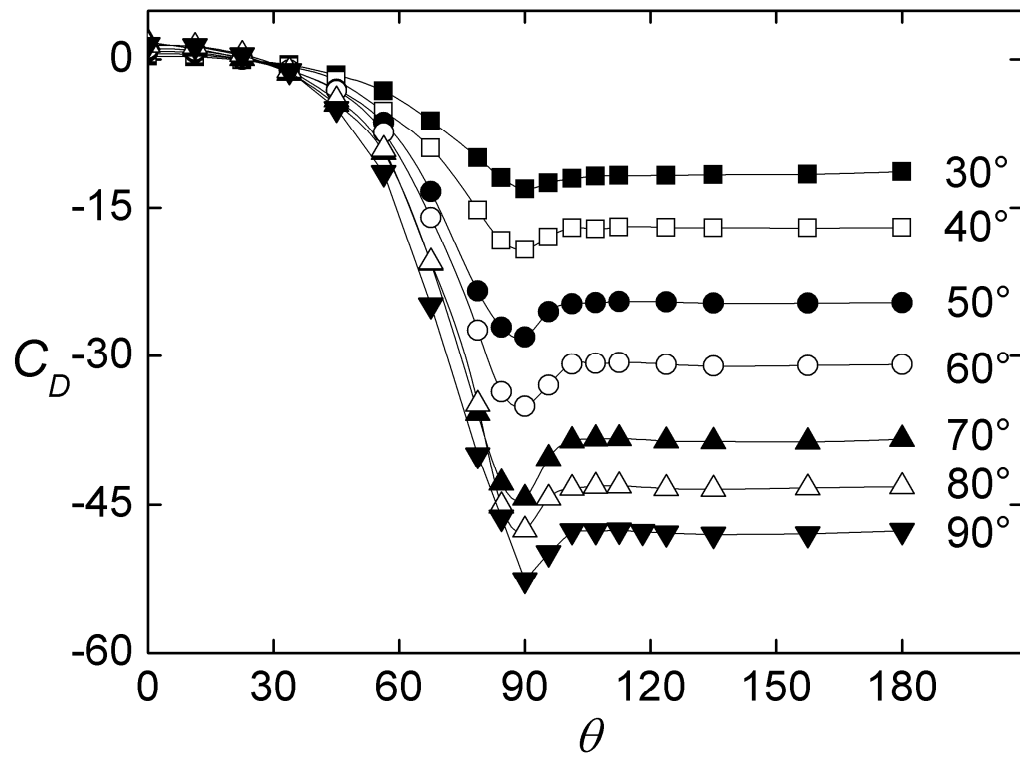


Figure 5: Polar profile of the pressure coefficient for  $Re = 4830$  (95 g/s). Each curve corresponds to inclination angles  $\alpha = 30, 40, 50, 60, 70, 80$  and  $90$  degrees respect to the incident direction.

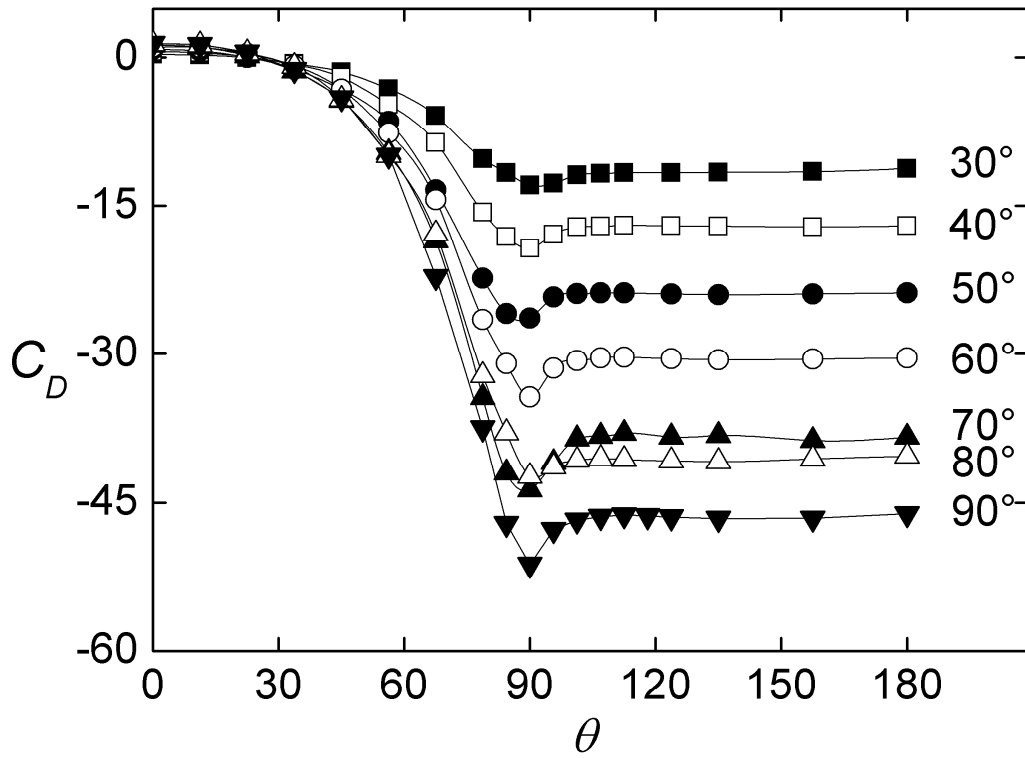


Figure 6: Polar profile of the pressure coefficient for  $Re = 6100$  (120 g/s). Each curve corresponds to inclination angles  $\alpha = 30, 40, 50, 60, 70, 80$  and  $90$  degrees respect to the incident direction.

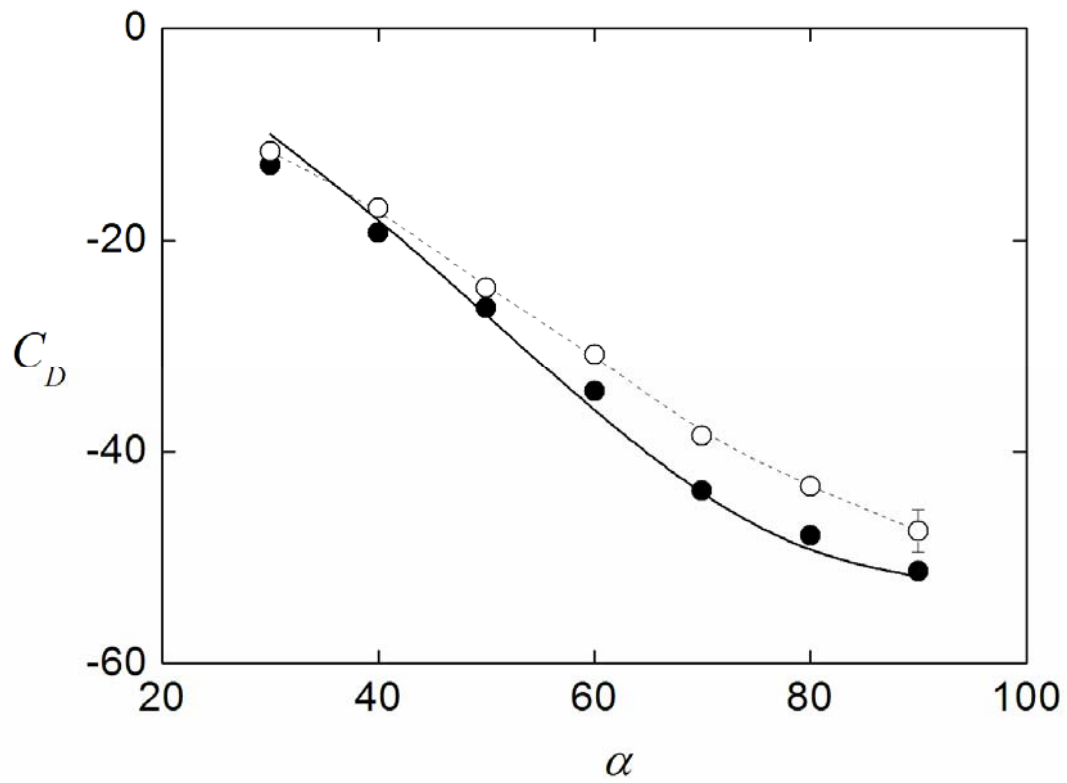


Figure 7. Dependence of the pressure coefficient at the rear ( $\circ$ ) and at  $\theta = 90^\circ$  ( $\bullet$ ) with the inclination angle. The error bar on the last symbol applies to all points.

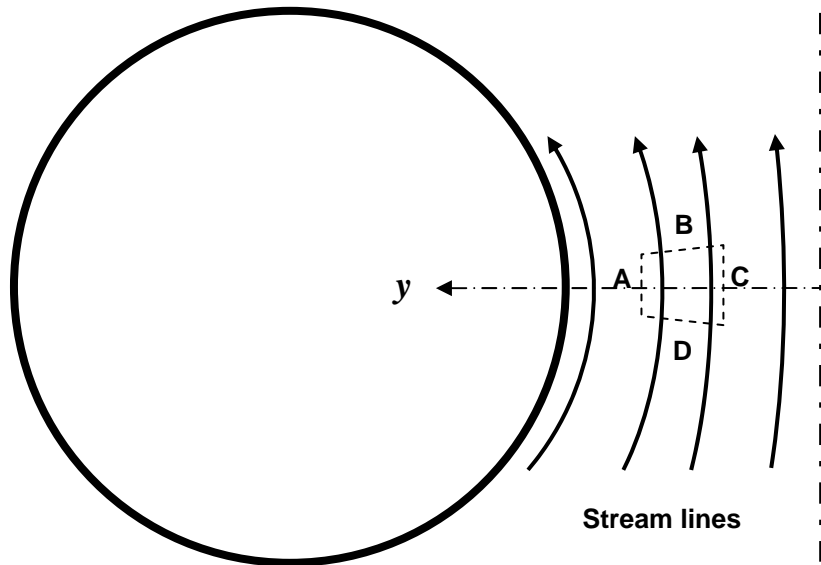


Figure 8. Control volume ABCD at the gap between bars. The pressure force at A is  $-(pR d\theta)$ . The pressure force at C is  $\left(p + \frac{\partial p}{\partial n} dn\right)(R + dn)d\theta$ . The pressure force projection in direction  $n$  at B and D is  $-(p dn d\theta)$ .

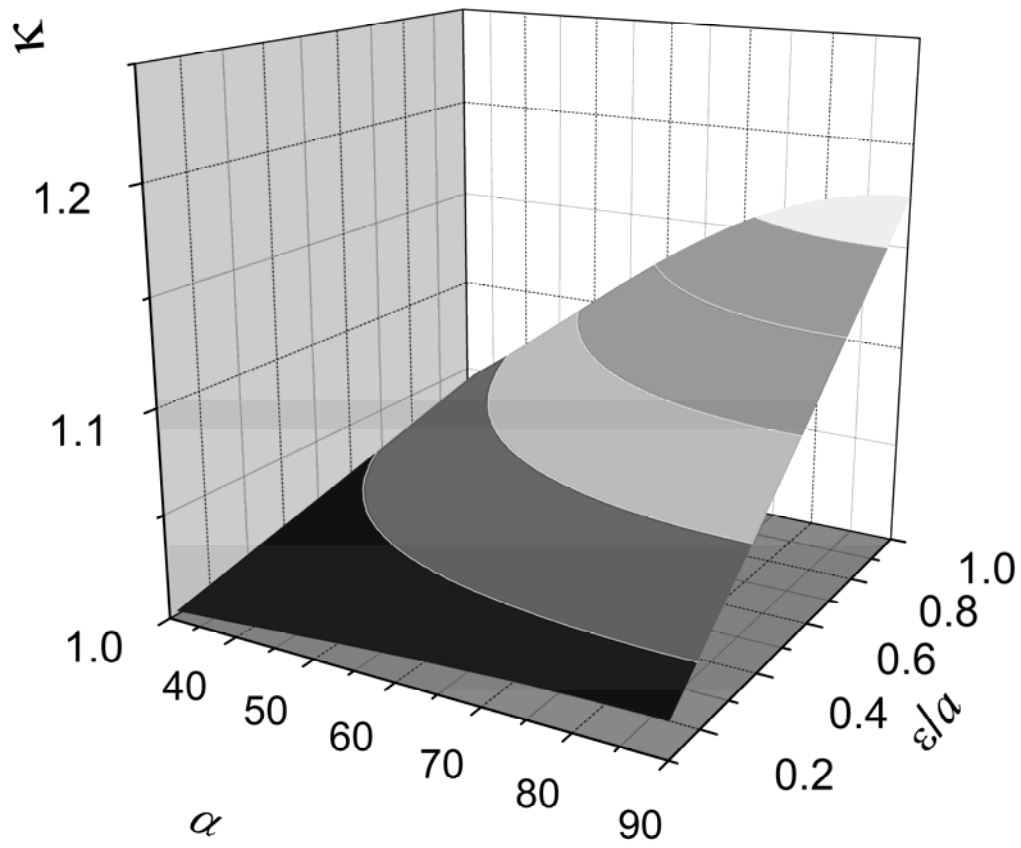


Figure 9. Geometrical correction factor given by Eq. (14)

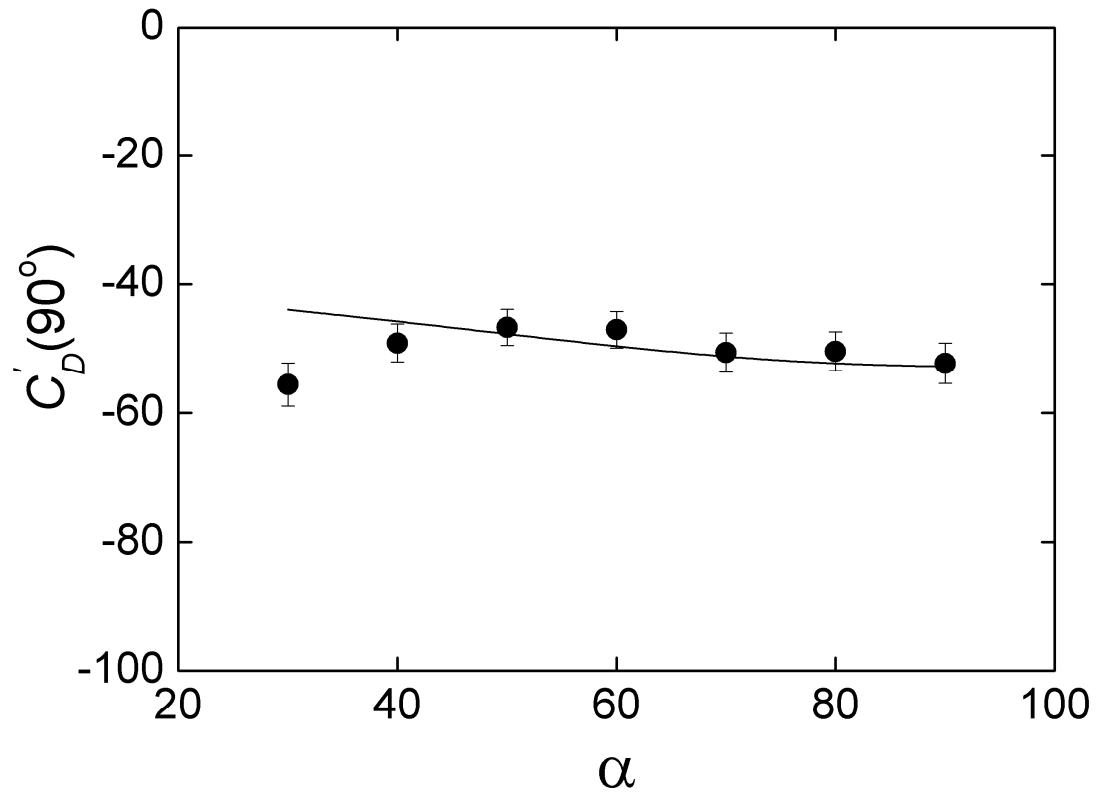


Figure 10. Pressure drop coefficient calculated with the velocity component normal to the cylinders axis.